Volume 8
Number 1
January 2021
Pages 1–286

Materials Horizons

rsc.li/materials-horizons

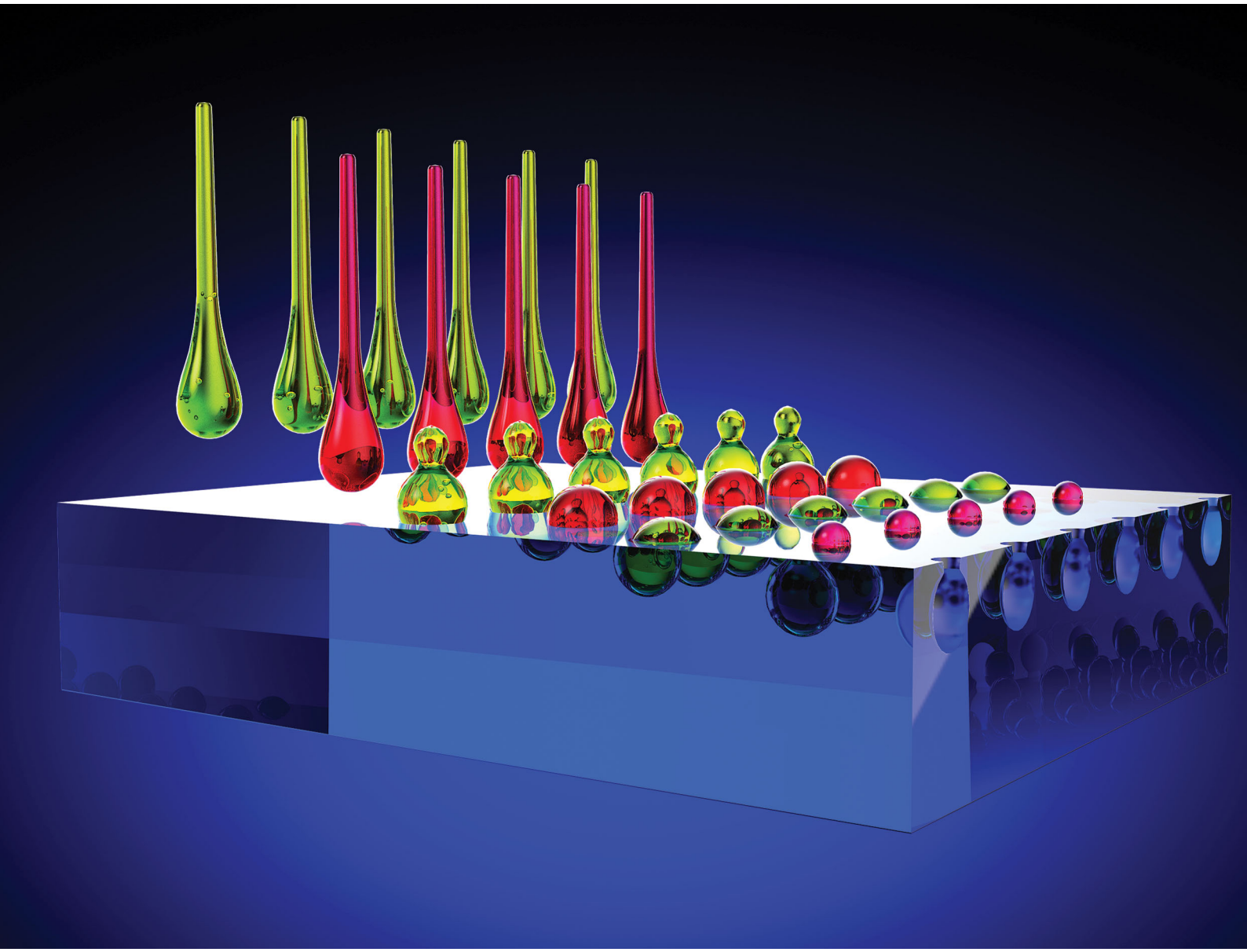

ISSN 2051-6347

ROYAL SOCIETY OF CHEMISTRY

COMMUNICATION
Qingxin Zhang, Ronan Daly *et al.*
Direct-writing microporous polymer architectures – print, capture and release

Materials Horizons

ROYAL SOCIETY OF CHEMISTRY

COMMUNICATION

View Article Online
View Journal | View Issue

Cite this: *Mater. Horiz.*, 2021, 8, 179

Received 9th September 2020,
Accepted 11th November 2020

DOI: 10.1039/d0mh01460e

rsc.li/materials-horizons

Direct-writing microporous polymer architectures – print, capture and release†

Qingxin Zhang, *[a] Niamh Willis-Fox, [a] Clare Conboy[b] and Ronan Daly *[a]

In the nature-inspired breath figure method, rafts of condensed water droplets self-organise and imprint into a permanent microporous polymer structure. This could have exciting applications in drug delivery, tissue engineering and sensors but it is extremely difficult to control or functionalise the final structure. Here, we show direct-writing of droplets onto fluid surfaces by inkjet printing as a breakthrough to dial-in a required pattern, structure and function into the polymer film.

New concepts

The core concept demonstrated here for the first time is the direct-writing of fluid droplets by inkjet printing into cross-linkable fluids. This delivers polymer materials with tuneable porosity, pore geometry, pore patterning and final functional properties. Each step of the process is examined, with demonstrations of (1) droplet stability due to interfacial energy balances, (2) non-coalescence phenomena upon drop–drop impact, (3) packing by self-organisation, (4) capturing of the droplets and (5) release of captured materials. Each is reported in turn and analysed using high frame rate imaging, microscopy and rheology. This approach is inspired by breath figure patterning, where micron-scale water droplets naturally condense at a polymer solution/air interface and then self-organise and imprint into a permanent microporous polymer structure. The work here is differentiated by tackling all of the main challenges to scaling up this original method, namely the sensitivity to local environmental conditions, the use of mostly harmful solvents and the complex post-processing to functionalize the imprinted pores in the breath figure method. Our research maintains the benefits of the breath figure method, while solving these challenges to enable future applications in sensing, filtration, drug delivery and high throughput screening.

1. Introduction

Creating functional pores with specific architectures within polymer materials is essential when designing for applications such as controlled release of drugs,[1] tissue engineering,[2,3] filtration,[4] catalysis[5] and sensors.[6] Pores may be formed and controlled across the surfaces of polymer materials or made to fill the bulk and form 3D open- or closed-cell foams. Diverse patterning techniques have been employed when precise structures or sizes are needed, such as lithography[7] and a range of approaches with direct templating.[8] One direct templating technique, known as the 'Breath Figure (BF) method', has received extensive attention over the last three decades.[9–13] This is a remarkable nature-inspired technique that relies on self-organisation and imprinting of condensed water droplets at a polymer solution surface. In the first step, a polymer solution of a highly volatile solvent is exposed to a high humidity gas flow. The solvent evaporates, which drives cooling of the liquid interface, onto which water droplets rapidly condense. In the second step, continued solvent evaporation drives rapid convection in the solution leading to self-organisation of the condensed droplets. Domains of ordered micron-scale droplets pack together across the polymer solution surface with many defects and some coalescence seen, mostly at domain interfaces. In a final third step, the rest of the solvent evaporates and the droplets are templated into the entangled polymer film, imprinting their shape to create porous structures. This technique has excited interest because it occurs rapidly at ambient temperatures and pressures and can deliver a wide range of architectures.[14,15] However, the dynamics of the formation process are very sensitive, with small fluctuations driving extreme changes in pore microstructure.[16] This sensitivity to local conditions and also to polymer concentration[17] continues to make this method empirical and extremely challenging to scale up for applications. In addition, the bulk of reported work relies on toluene, chloroform, carbon tetrachloride and carbon disulphide to drive this technique, which limit the end applications due to toxicity of the trapped solvent. Finally, the method is limited to templating by condensed water droplets only,

[a] *Institute for Manufacturing, Department of Engineering, University of Cambridge, UK. E-mail: qz250@cam.ac.uk, rd439@cam.ac.uk*
[b] *Printed Electronics Ltd., Amphenol Invotec Building, Hedging Lane, Tamworth, Staffordshire, UK*

† Electronic supplementary information (ESI) available. See DOI: 10.1039/d0mh01460e

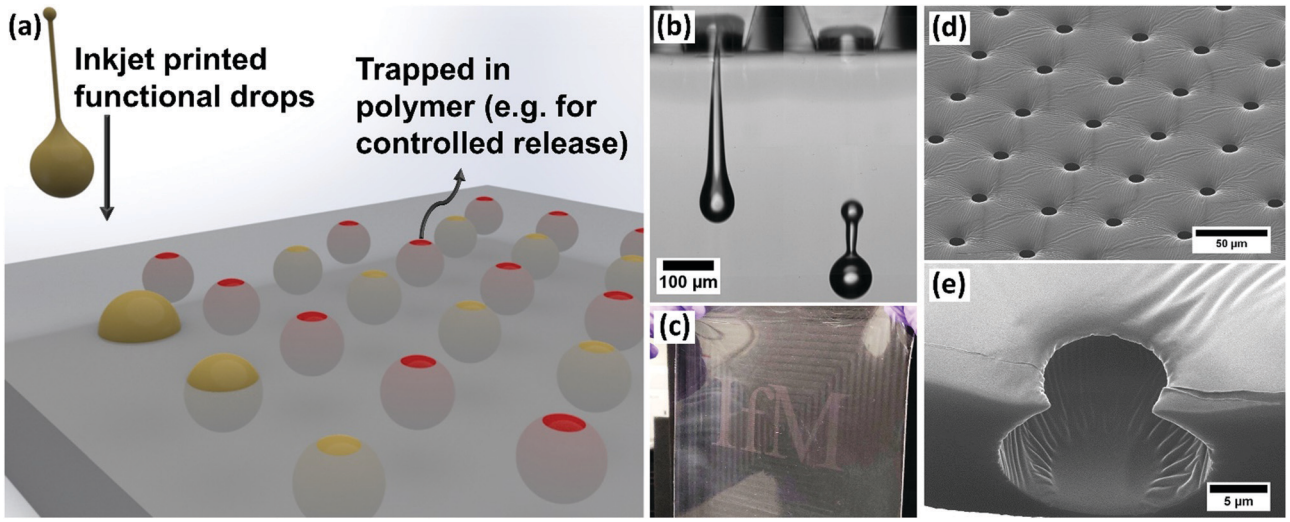

Fig. 1 (a) Illustration of the formation of microstructured polymer material, printing functional materials to a fluid for encapsulation to act as a template for a cross-linking polymer, (b) inkjet printed drops for delivery of fluids to a fluid surface, (c) an example of a test area of printed food dye, encapsulated in fully cured polymer and released later through diffusion from the pores, (d) electron microscopy image of a cured, microstructured PDMS surface, (e) image using helium ion microscopy of a cross-sectioned pore after the printed drop is removed.

leading to multiple steps if the final porous material needs to be functionalised.[14]

In this paper, we demonstrate a breakthrough approach of fluid-on-fluid templating that addresses all of these challenges and enables rapid fabrication of functional, structured polymer films making these applications feasible and scalable. Extrusion of fluids within the bulk or on the surface of an elastomer matrix has been pioneered[18–20] to show the ability to capture and control functional materials in macro-scale patterns. Inspired by the BF method, we use the highly controlled, tuneable, direct-write benefits of drop-on-demand (DoD) inkjet printing to controllably print micron-scale droplets to a fluid surface, as illustrated in Fig. 1(a). We show that in comparison to the original BF method this process delivers improved stability, improved control over coalescence, new controls over droplet packing and the ability to imprint a structure into a solvent-free biocompatible cross-linked polymer material. Functional material printing (shown in Fig. 1(b)) means we can dramatically improve the patterning and broaden the range of functional materials delivered to, trapped in and released from polymer films (Fig. 1(c)), with excellent control over pore volume or structure (Fig. 1(d) and (e)) for a wide range of applications.

2. Results and discussion

2.1 Controlled droplet deposition on liquid surfaces

Inkjet printing fires droplets directly to a surface and the content of the drops can be formulated to contain a wide range of functional materials while still printing reliably.[21,22] This process is highly programmable, with the droplet size and the pattern of the droplets delivered to the substrate easily controlled. The volume of each droplet is tuned through the choice of nozzle and the printing waveform.[21] These advantages are in stark contrast to the BF method in which water droplets condense and grow across the entire surface of polymer solution simultaneously and the final geometry of the porous polymer material is dependent on the original polymer concentration, the relative humidity and air flowrate.[13,23,24] Condensation and growth of droplets during the BF method also leads to coalescence, polydispersity of the structures and very poor repeatability across experimental systems.[25,26] In this study, to examine droplet deposition *via* DoD inkjet printing and subsequent drop–drop and drop–surface interactions, experiments were carried out by printing with a model fluid of 50%$_{w/w}$ glycerol in water, with a viscosity of 6.3 mPa s and surface tension of 69.2 mN m^{-1}. This formulation is commonly used as a model fluid for inkjet printing and is especially appropriate for translation to applications in biological and pharmaceutical printing. Experiments used Microfab printheads and printing parameters were always tuned to give single, repeatable drops, as shown in ESI,† Fig. S1. Glycerol was included to improve printability by increasing viscosity and reducing vapour pressure, while still maintaining the ink's Newtonian behaviour and high surface tension.

High speed imaging was used to examine the impact of microscale droplets on liquid surfaces. Representative stills from the captured videos at various times during droplet deposition are shown in Fig. 2. To vary drop impact conditions, the waveform amplitude was varied for each nozzle diameter tested (30–80 μm diameters). The study only used results where a single drop could be printed consistently without spray or small satellite drop formation, as shown in Fig. 1(b). The diameters of water/glycerol droplets studied varied from 50.8 ± 1.5 μm to 103.6 ± 3.0 μm and the speed of the droplets were tuned between 0.8 ± 0.1 m s^{-1} to 7.4 ± 0.7 m s^{-1}. As a direct comparison with the BF method, the model solution was first printed onto octyl

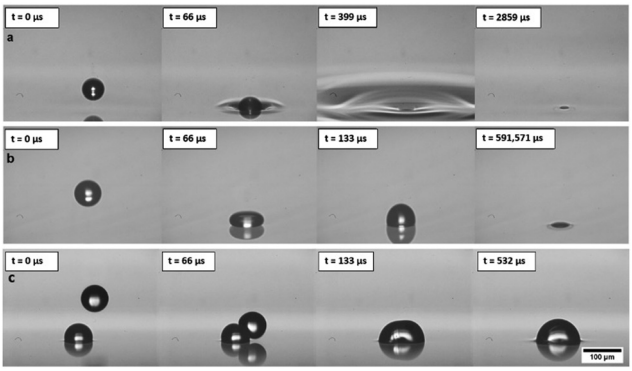

Fig. 2 Comparison of impact of 50%$_{w/w}$ glycerol water droplets impact behaviour on (a) octyl acetate and (b) and (c) PDMS. Droplet diameter in (a) is approximately 71.3 µm, the velocity of the droplet before hit the surface is 1.1 m s^{-1}. Droplet diameter in (b) is approximately 91.7 µm, the velocity of the droplet before hitting the surface is 1.9 m s^{-1}. (c) When printing a second drop to PDMS before the first drop has imbibed, impact and coalescence occurs.

acetate (OA), an organic solvent with near identical properties to solvents commonly used in that method.[27] The recorded impact behaviour is shown in Fig. 2(a).

We immediately found that this new approach to capturing droplets is extremely robust, with the full range of drop sizes and velocities never leading to splashing of the liquid substrate and always leading to droplets imbibed within a few hundred microseconds. The behaviour of inkjet printed microscale drops is dominated by surface tension forces and they always remain as spherical caps at a fixed and characteristic contact angle[27] pinned at the fluid–air interface. Droplets never submerge fully into the bulk of the solution upon impact, showing improved stability compared with condensation techniques. Once at their pinned location, droplets do not sink, despite the differences in density, as surface tension forces dominate over buoyancy at this scale. This behaviour is repeatable for all direct printing conditions attempted for octyl acetate and demonstrates a stable and repeatable process. The characteristic contact angle of droplets observed in octyl acetate surface is 163°.

The solvents required for the BF method are mostly harmful and toxic, and in a step towards removing the need for these solvents, we examined printing directly to a crosslinkable fluid polymer system, polydimethylsiloxane (PDMS). The panels in Fig. 2(b) show the drop impact behaviour and slower imbibing time on the PDMS surface.

The characteristic contact angle was challenging to observe in this case but is $>163°$. The dramatically higher viscosity of PDMS changes this deposition behaviour, with the droplet impacting as if on a solid surface. Importantly, the final outcome is not affected and droplet imbibing does still occur, albeit over a longer time. The droplets take $\sim$0.5 s to flow into the liquid surface but still remain pinned to the underside of the interface. Industrial inkjet printing processes normally create droplets at 10 s of kHz, and so considering the time taken for droplets to flow into the liquid, in this case the next printed drop will land long before the first drop has imbibed below the surface. As can be seen in Fig. 2(c), if the spacings are not correct then droplets interact above the liquid substrate and coalescence occurs. Once droplets coalesce, they still imbibe below the fluid surface to the same contact angle, dramatically altering the pore dimensions and the final pattern structure through the introduction of defects. Thus, this coalescence upon contact above the liquid/air interface determines the limit of packing density if the timings or spacing is not controlled during printing. Merging of printed droplets may also be an important consideration when droplets interact within the liquid substrate and so coalescence must be examined to show the maximum feasible packing density for controlled, reliable patterning.

2.2 Drop–drop interactions and controlling coalescence

The original BF method relies heavily on the non-coalescence phenomenon[28] where droplets have been observed to pack tightly together and remain separate both in pure solvent and polymer-containing systems. This makes it possible to pack drops together and form the remarkable micro and nanostructures observed. It is not clear if this is due to thermocapillary convection,[29] a lubricating flow of evaporating solvent,[10] the control of convection currents[30] or a combination of these influences. Droplet coalescence occurs in this direct-printing technique when a printed droplet impacts a second drop already sitting above the liquid. It is unclear what behaviour to expect when printing to a drop that has already imbibed or when two drops interact below the surface. To probe this, droplets were printed directly onto the liquid surfaces of firstly octyl acetate and secondly PDMS. The droplets were allowed to imbibe to their characteristic contact angle below the liquid surface. A second droplet was then printed at a range of fixed spacings away from the first droplet (as illustrated in Fig. 3(a)) and the coalescence/non-coalescence behaviour was recorded by high speed imaging.

The relative distance (d_r) is designated as the distance between the centres of the two drops (d_s), divided by the diameter, d, ($d_r = d_s/d$). This means, for $d_r < 1$, the droplet spacing is sufficiently small that there is definite impact between the two droplets. This was carried out for a wide range of droplet spacings. It is shown in Fig. 3(a) that both coalescence and non-coalescence behaviours are observed upon drop–drop impact for both OA and PDMS. For head-on drop–drop impact, coalescence was observed. Incredibly, at larger spacing the printed drop impacts and slides off the submerged drop, avoiding any coalescence. However, at a distance where the drop-to-drop spacing is approximately the same as the drop radius, there is a transition to coalescence behaviour.

Rather than a sharp transition, a region is identified where droplet behaviour is difficult to predict (d_r of 0.58–0.71 for octyl acetate, and 0.53–0.58 for PDMS, as shown in Fig. 3(a)). Fig. 3(b) shows both coalescence and non-coalescence behaviour when water/glycerol droplets are printed to octyl acetate surfaces, with drop–drop impact in both cases. However, the behaviour is highly repeatable outside of these regions. As there is no evaporation or temperature difference in this case, non-coalescence is occurring due to a lubrication layer between the two drops.

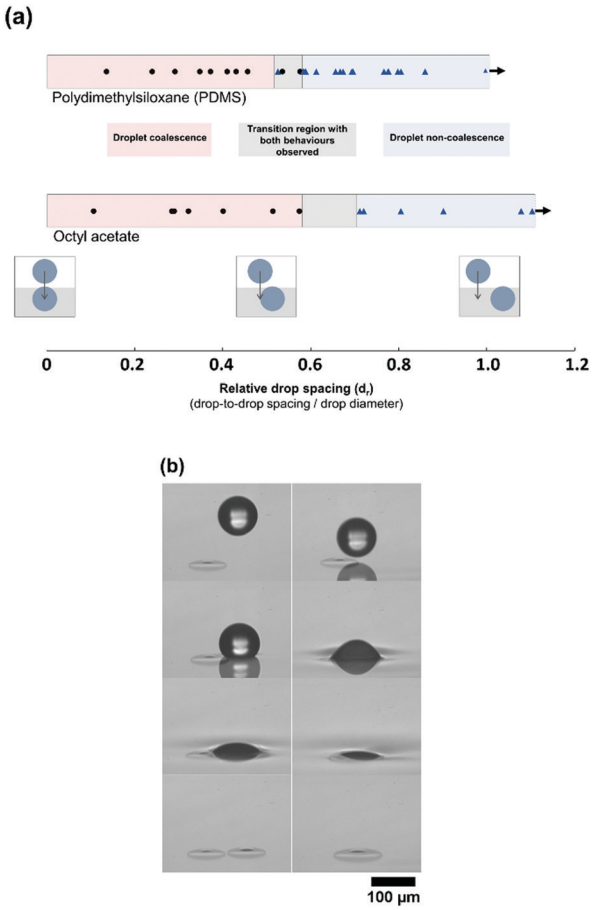

Fig. 3 Drops (50%$_{w/w}$ glycerol/water) were printed with a range of different spacings onto octyl acetate and PDMS. Data points for experiments recorded are shown, with shading to define the regions of coalescence and non-coalescence for each fluid. (a) Drops coalesce after printing onto both fluids at very small drop-to-drop spacing, there is a transition region and then non-coalescence phenomena are observed upon drop impact. (b) Images are captured showing both coalescence and non-coalescence behaviour for printing to an octyl acetate surface.

When the printed droplet makes contact with the small volume of water/glycerol protruding from the fluid surface due to the first drop, then there is no lubrication layer and coalescence can occur. Therefore, the stability of droplets and their coalescence behaviour upon impact is believed to be related to the contact angle formed by the drops within the bulk fluid, that determines this protruding volume.[27] There may be times when there is a benefit to driving coalescence, for example if tuning the volume of the embedded droplet. However, because the coalescence appears only to occur when the impinging droplet contacts the part of the first droplet protruding from the liquid surface, the precision of printing will be the key factor when aiming to control non-coalescence. This level of accuracy is known to be very challenging at industrial speeds[31] and the work here explores an alternative route to achieving high-density packing of individual drops, inspired by the BF method. We examine increasing the spacing of printed drops to avoid any direct drop–drop contact followed by self-organisation to drive droplet packing.

2.3 Convection-driven droplet self-organisation

Self-organised packing of condensed droplets by the BF method relies heavily on convection, driven by the temperature drop from solvent evaporation.[16] As mentioned, here we are moving away from the harmful solvents needed to achieve this and so we explore the feasibility of convection-driven self-organisation in PDMS, with the goal of crosslinking the polymer and trapping droplets. To achieve this, a miniature heated plate was used to heat a well (~5 ml) of PDMS from below. The well was approximately 9 mm deep, with the droplets printed to the upper surface. Shadowgraphy imaging of the droplets was used to monitor any movement, with the detailed experimental setup and validation of convection currents described in the ESI,† Fig. S2. Water/glycerol droplets were inkjet printed to the PDMS using a Dimatix Materials Printer 2850 for these experiments, with an approximate droplet diameter of 20 μm. This printer was chosen to enable printing of significantly larger droplet arrays than the Microfab system discussed above. An area of 10 mm × 10 mm was printed on the PDMS surface, with a droplet spacing of 50 μm to ensure no drops can come into contact at this stage. Within this area, the patterns were printed as square arrays, as shown later in this publication.

We immediately observed convection and self-organisation commencing once an elevated temperature was applied from below. For the work reported here we used a standard heating temperature of 80 °C to ensure rapid convection and sample preparation. We are significantly above the critical Rayleigh number and so anticipate a Rayleigh–Bénard convection mechanism. A downward flow near the centre of the well is observed and flow at the surface from the edge towards the centre, leading to an evenly contracting printed pattern and hence droplet packing. Self-organisation is seen to drive the pattern of droplets from the original 10 mm wide square printed area to a square approximately 3.5 mm in diameter. The droplets are packed into close contact through convection, with the samples here packing completely in ~3 minutes, as shown in Fig. 4. Details are provided in ESI,† Fig. S2 on the experiments built to demonstrate these convection currents and showing the effect on droplet packing.

Once the droplets are close enough to interact, there is a marked difference between the behaviours of the two printed patterns (square or hexagonal printed). Droplets initially printed

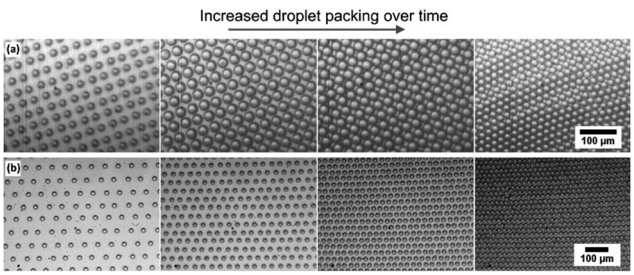

Fig. 4 Droplet packing on PDMS by convection-driven self-organisation. (a) Square arrays printed, with packing leading to defects. (b) Hexagonal arrays printed with packing leading to minimal defects.

in a square pattern continue to shift, with lines of droplets rolling past each other, because the system is clearly not at minimum packing energy. This leads to dislocations (Fig. 4(a)), reminiscent of those seen in the breath figure literature in systems that were not given sufficient time to pack, or were packed in a highly non-equilibrium system such as on tilted or spin coated samples.[12,32] Changing to a hexagonal printed pattern instead gives an ideal hexagonal close-packed final array (Fig. 4(b)). The spacing between droplets remains equal as they pack, coming into contact and remaining in a 'single crystal' packing format over the full area. This level of order has never been achieved with the alternative BF droplet self-organisation techniques and offers a major development in control. To capitalise on this unprecedented level of control, we then examined trapping and templating these droplets to form imprints into the polymer material.

2.4 Droplet capture and imprinting

Droplet capture and imprinting always previously relied on a polymer precipitating at the solution/droplet interface, followed by a gradual entanglement of polymer in the bulk solution to finally capture the templating droplets.[33] Here, we capture and imprint droplets by crosslinking the PDMS network through addition of a crosslinking agent. This approach has a number of advantages, such as the significant improvement in mechanical properties of the final film due to the cross-linking and also the fact that this process can occur at room temperature, or be triggered/accelerated by using elevated temperatures.

The use of an elevated temperature to accelerate the cross-linking was chosen here to enable a single step process that both drives convection and also templates the droplets to create the pores. Examples of droplet patterns captured in crosslinked PDMS are shown in Fig. 5 and 6 for both square and hexagonal patterns. To-date, this is the only reliable way reported to programme and capture square array patterns with fluid based templating techniques.

With the understanding that the self-organisation is convection dependent, the temperature gradient across the PDMS depth and also the bulk viscosity will be determining factors in droplet movement.[34] The role of temperature and viscosity on self-organisation and templating in PDMS was therefore investigated. With the initial mixing of PDMS and crosslinker marked as the starting point of any experiment, PDMS begins to crosslink immediately at room temperature. Rheological analysis shows the viscosity at set times after mixing between 1 hour (3.25 Pa s) and 10 hours (15.20 Pa s) after mixing (Fig. 5(a)). Patterning was carried out at room temperature on each of these samples, and then an increase in temperature (80 °C) was applied to drive self-organisation and crosslinking. To give a representative rheological study, a temperature of 80 °C was applied after 300 s during rheological measurements of these samples, as shown in Fig. 5(a).

As soon as the elevated temperature is applied, there is an initial decrease in viscosity as expected for a polymer system, and then a dramatic increase due to the acceleration in crosslinking.

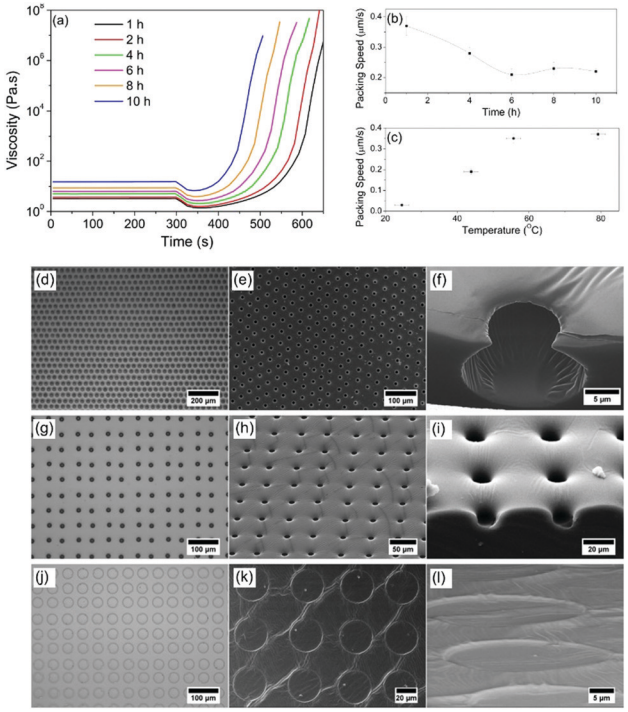

Fig. 5 (a) PDMS rheology after leaving it to cross-link for 1 h to 10 h. In each case, PDMS is at room temperature for 300 s. It is then increased to 80 °C, mimicking the process in which the printed samples were treated. (b) Drop self-organisation speed on PDMS while convection happens. Packing speed slows down when PDMS is cured for longer time. (c) Packing speed increases as the temperature applied for convection increases. (d) 50%$_{w/w}$ glycerol/water solutions are printed and captured in PDMS, optical microscopy image of patterned PDMS. (e) Electron microscopy image of the same sample, (f) neon ion milled cross-section of imprinted structure. (g)–(i) Optical, SEM and cross-section of PDMS, cured for 10 h at room temperature, (j)–(l) Optical, SEM and cross-section of PDMS, cured for 24 h at room temperature.

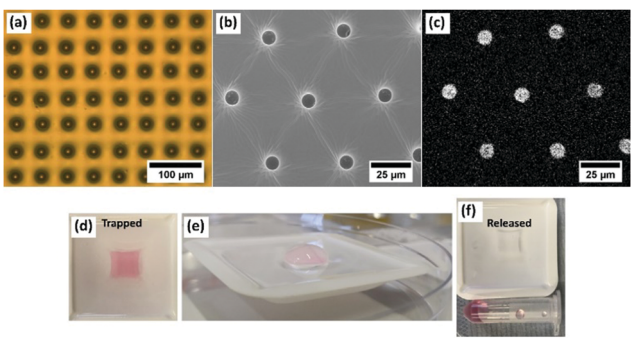

Fig. 6 (a) Optical microscope image of printed PEG 1000 trapped in PDMS, (b) electron microscopy image of iron oxide nanoparticle inks trapped in PDMS, (c) EDX signal of Fe for the same printed sample showing functionalised internal surface, (d) a red food dye is included in the printed patterns and trapped in PDMS, (e) after a day water is added to show release of the pseudo-functional ink, (f) the final collected sample contains the food dye and the printed structure is emptied.

Fig. 5(b) shows that droplet packing speeds at 80 °C are reduced for patterning after longer initial curing times. Fig. 5(c) shows

that for a fixed curing time (in this case 1 hour), droplet packing speed increases with temperature (due to the increase in convection current speed). By using these new controls over the extent to which the droplets will be able to pack, the system has become dramatically more repeatable and tuneable.

For the first time, droplets can be deliberately packed and stabilised in hexagonal or square arrays, and a direct-write free design can be used, as shown in Fig. 1 and 5. Additional images highlighting this control are provided in the ESI,† Fig. S2-1–S2-4. When examining the porous architecture in detail, it is found that the time of patterning following initial curing time is a critical factor in the final imprint shape. Fig. 5(d)–(f) shows as an example optical and SEM images of a standard sample templated with a hexagonally packed pattern using our model fluid printed onto PDMS, 8 h after mixing with crosslinker. It is clear that even after this long curing period, despite the increased viscosity observed in Fig. 5(a), droplets still imbibe into the PDMS and self-organisation and packing takes place. The cross-section carried out with neon ion milling (Fig. 5(f)) reveals a small opening on the surface and a wider spherical chamber under the surface. These spherical pores are also found in all samples that are pre-cured for less than 8 hours also. However, droplet patterning in a square array after 10 h curing (Fig. 5(g)–(i)) shows the shape of the imprints changes from spherical to short cylindrical pits (Fig. 5(i)).

Drops imbibe but are captured rapidly before they can create standard spherical shapes. At 24 h curing time, PDMS has almost fully cured by the time printed droplets are deposited but it still has the ability to be shaped by droplets. The square array pattern is again used in this example (Fig. 5(j) and (k)). Upon close inspection, it can be seen that the droplets never imbibe into the surface. Instead, they remain above the surface similar to landing on a solid surface. There is some limited flow of the polymer to leave only shallow, nanoscale 'footprints' (Fig. 5(l)). Tuning packing structures and porous architectures opens up this direct-write approach to a broad range of new applications.

2.5 Beyond breath figures to applications

Direct deposition of fluid enables the droplet templating technique to finally be a tuneable and scalable process with the inclusion of functional materials at the same time as the templating. Drug delivery is more often carried out through the breakdown of materials such as polyethylene glycol (PEG) and so PEG1000 was inkjet printed directly to the surfaces and captured as droplets using the same technique (Fig. 6(a)). Functionalisation of the inner surface of the imprints was demonstrated using a range of proteins and nanoparticles, with the example of trapping iron oxide nanoparticles shown in Fig. 6(b), with the EDX signal in Fig. 6(c). As an initial demonstration, red food dye was included in a printed pattern and embedded in PDMS. A day later, upon addition of an aqueous medium, the pores are emptied as the dye is released through diffusion. Current work is exploring specific drug delivery applications into biological sample.

3. Discussion and conclusions

Combining direct-write inkjet printing with the principles of the nature-inspired BF method provides an unprecedented and robust way of delivering known functionality to porous microstructures with minimal defects in the final material. Each of the key steps of the BF method has provided inspiration for this work. The stability of printed drops fired at fluid/air interfaces is studied and found to be equivalent to that noted in the literature for gentle droplet growth by condensation. This is an intriguing finding that suggests there may be a feasible approach to combine the two approaches to deliver multiscale structures or to further grow or shrink the deposited droplets by tuning the vapor–liquid–equilibrium. Non-coalescence phenomena still rely on avoiding direct contact between printed drops through the presence of a slow-draining, immiscible fluid. There is a limitation to inkjet printing because of the drop positioning accuracy, which can lead to unexpected contact and coalescence behaviour, and so self-organisation was explored as a gentle way of bringing droplets closer together. This is found to be a more reliable and repeatable way of ensuring near-perfect droplet packing. The convection is driven by an inverted temperature gradient, compared with evaporation-based self-organisation and is likely going to break down for very viscous fluids or when the film thickness is reduced.

Any digitally-controlled drop-based pattern can be delivered, and we show the microstructure of pores can also be tuned based on the printing pattern and polymer viscosity. Control of the viscosity is not something explored in the BF method, but here adds not only to the control of the geometry but also the ability to stabilise non-equilibrium packing, such as a square array. Future work will focus on the detailed surface energy balance to better control the relative volumes below and above the liquid/air interface, and will also study further the inclusion of other polymers and embedded drugs for analysis of delivery control. This dramatic improvement in manufacturability and control of these polymer structures paves the way for rapid translation to applications in combination drug delivery and drug delivery coating development.

4. Materials and methods

4.1 Studying impact of droplets fluid surfaces

Video was captured of droplets landing on octyl acetate (99+%, Acros Organics) and PDMS (Sylgard® 184 silicone elastomer kit, Dow Corning) fluid surfaces, using a Phantom® v7.3 high-speed camera. MicroFab printhead MJ-ABP-01 series nozzles were used to print 50%$_{w/w}$ glycerol in water. Glycerol (99+% extra pure, Acros Organics) and water of analytical reagent grade were used to prepare the printing solution. Solutions were filtered with a syringe filter (hydrophilic PTFE, 0.45 μm) prior to printing.

4.2 Studying droplet stability on fluid surfaces

One drop of 50%$_{w/w}$ glycerol/water solution was printed onto the fluid surface, then the substrate stage was adjusted manually with

a high precision x–y–z stage and a second drop printed, while capturing the video of the second drop using Phantom® v7.3 high-speed camera. ImageJ software was used to analyse the distance between the droplets and the diameter of the droplets.

4.3 Wide-area patterning of PDMS

To prepare the PDMS used for patterning, the base of PDMS was mixed with the crosslinker at a 10 : 1 ratio by volume. Significant manual mixing was carried out for 10 min. Approximately 5 ml PDMS was transferred into a number of plastic weighing boats (dimensions 43 mm × 43 mm × 9 mm) and these were degassed with a vacuum pump until there were no bubbles remaining. After a set curing time, the printing was carried out with the Dimatix Materials Printer (DMP-2800, Fujifilm). PDMS was placed directly onto the hot metal tray of an 80 °C oven directly after printing. This drives convection-based self-organisation and packing and ensures complete crosslinking within 2 hours. Patterning was carried out by printing the glycerol/water solution noted earlier and also by printing PEG 1000 (Sigma Aldrich) while heated to 60° to ensure printability.

4.4 Convection and droplet self-organisation

PDMS rheology was studied using an Anton Paar MCR 302 rheometer. After mixing of the two components, to ensure onset of curing, samples were degassed and left at room temperature for 1 h, 2 h, 4 h, 6 h, 8 h, and 10 h. The self-organisation and packing of printed drops were analysed for each sample and interpreted based on rheological analysis. The samples for convection study were prepared in a pre-made glass-bottomed weighing boat. A Procilica CV1280C camera was used to capture the convection video. A metal stage with a 10 mm × 10 mm hole was fixed on a Peltier heater to provide constant heating while allowing light from an LED to pass through the hole and the cover slip so that the drops on PDMS could be recorded by shadowgraphy. A diagram of this setup and more details validating the convection studies are detailed in the ESI,† Fig. S2.

Conflicts of interest

There are no conflicts to declare.

Acknowledgements

We would like to acknowledge the support of the Cambridge Trust, BBSRC (BB/T011750/1) and EPSRC (EP/S009000/1), each for supporting this work.

References

1 G. Vilar, J. Tulla-Puche and F. Albericio, Polymers and Drug Delivery Systems, *Curr. Drug Discovery*, 2012, **9**, 367–394.
2 B. Yao, Q. Zhu, L. Yao and J. Hao, Fabrication of honeycomb-structured poly(ethylene glycol)-*block*-poly(lactic acid) porous films and biomedical applications for cell growth, *Appl. Surf. Sci.*, 2015, **332**, 287–294.
3 Y. Zhu, *et al.*, Honeycomb-Structured Films by Multifunctional Amphiphilic Biodegradable Copolymers: Surface Morphology Control and Biomedical Application as Scaffolds for Cell Growth, *ACS Appl. Mater. Interfaces*, 2011, **3**, 2487–2495.
4 J. Mansouri, E. Yapit and V. Chen, Polysulfone filtration membranes with isoporous structures prepared by a combination of dip-coating and breath figure approach, *J. Membr. Sci.*, 2013, **444**, 237–251.
5 I. Pulko, J. Wall, P. Krajnc and N. R. Cameron, Ultra-High Surface Area Functional Porous Polymers by Emulsion Templating and Hypercrosslinking: Efficient Nucleophilic Catalyst Supports, *Chem. – Eur. J.*, 2010, **16**, 2350–2354.
6 M. S. Silverstein, H. Tai, A. Sergienko, Y. Lumelsky and S. Pavlovsky, PolyHIPE: IPNs, hybrids, nanoscale porosity, silica monoliths and ICP-based sensors, *Polymer*, 2005, **46**, 6682–6694.
7 Y. Xia, J. a. Rogers, K. E. Paul and G. M. Whitesides, Unconventional Methods for Fabricating and Patterning Nanostructures, *Chem. Rev.*, 1999, **99**, 1823–1848.
8 D. Wu, *et al.*, Design and preparation of porous polymers, *Chem. Rev.*, 2012, **112**, 3959–4015.
9 B. B. Franqois, O. Pitois and J. Franqois, Polymer Films with a Self-organized Honeycomb Morphology, *Adv. Mater.*, 1995, 8–11.
10 M. Srinivasarao, D. Collings, A. Philips and S. Patel, Three-dimensionally ordered array of air bubbles in a polymer film, *Science*, 2001, **292**, 79–83.
11 G. Widawski, M. Rawiso and B. François, Self-organized honeycomb morphology of star-polymer polystyrene films, *Nature*, 1994, **369**, 387–389.
12 A. Bolognesi, *et al.*, Self-organization of polystyrenes into ordered microstructured films and their replication by soft lithography, *Langmuir*, 2005, **21**, 3480–3485.
13 R. Daly, J. E. Sader and J. J. Boland, The dominant role of the solvent–water interface in water droplet templating of polymers, *Soft Matter*, 2013, **9**, 7960.
14 J.-P. Gao, *et al.*, Well-defined monocarboxyl-terminated polystyrene with low molecular weight: A candidate for the fabrication of highly ordered microporous films and microspheres via a static breath-figure process, *Eur. Polym. J.*, 2014, **59**, 171–179.
15 S. Zhai, J.-R. Ye, N. Wang, L.-H. Jiang and Q. Shen, Fabrication of porous film with controlled pore size and wettability by electric breath figure method, *J. Mater. Chem. C*, 2014, **2**, 7168.
16 R. Daly, J. E. Sader and J. J. Boland, Taming Self-Organization Dynamics to Dramatically Control Porous Architectures, *ACS Nano*, 2016, **10**, 3087–3092.
17 M. H. Stenzel, C. Barner-Kowollik and T. P. Davis, Formation of honeycomb-structured, porous films *via* breath figures with different polymer architectures, *J. Polym. Sci., Part A: Polym. Chem.*, 2006, **44**, 2363–2375.
18 L. Cai, J. Marthelot, C. Falcón, P. M. Reis and P. T. Brun, Printing on liquid elastomers, *Soft Matter*, 2020, **16**, 3137–3142.

19 L. Cai, J. Marthelot and P. T. Brun, An unbounded approach to microfluidics using the Rayleigh–Plateau instability of viscous threads directly drawn in a bath, *Proc. Natl. Acad. Sci. U. S. A.*, 2019, **116**, 22966–22971.
20 A. Z. Nelson, B. Kundukad, W. K. Wong, S. A. Khan and P. S. Doyle, Embedded droplet printing in yield-stress fluids, *Proc. Natl. Acad. Sci. U. S. A.*, 2020, **117**, 5671–5679.
21 I. M. Hutchings and G. D. Martin, *Inkjet Technology for Digital Fabrication*, John Wiley & Sons, Ltd, 2012.
22 R. Daly, T. S. Harrington, G. D. Martin and I. M. Hutchings, Inkjet printing for pharmaceutics – A review of research and manufacturing, *Int. J. Pharm.*, 2015, **494**, 554–567.
23 J. Peng, Y. Han, Y. Yang and B. Li, The influencing factors on the macroporous formation in polymer films by water droplet templating, *Polymer*, 2004, **45**, 447–452.
24 A. Zhang, H. Bai and L. Li, Breath Figure: A Nature-Inspired Preparation Method for Ordered Porous Films, *Chem. Rev.*, 2015, **115**, 9801–9868.
25 a Limaye, R. Narhe, A. Dhote and S. Ogale, Evidence for Convective Effects in Breath Figure Formation on Volatile Fluid Surfaces, *Phys. Rev. Lett.*, 1996, **76**, 3762–3765.
26 L. Heng, B. Wang, M. Li, Y. Zhang and L. Jiang, Advances in fabrication materials of honeycomb structure films by the breath-figure method, *Materials*, 2013, **6**, 460–482.
27 R. Daly, J. E. Sader and J. J. Boland, Existence of Micron-Scale Water Droplets at Solvent/Air Interfaces, *Langmuir*, 2012, **28**, 13218–13223.
28 A. Steyer, P. Guenoun and D. Beysens, Hexatic and fat-fractal structures for water droplets condensing on oil, *Phys. Rev. E: Stat. Phys., Plasmas, Fluids, Relat. Interdiscip. Top.*, 1993, **48**, 428–431.
29 U. H. F. Bunz, Breath Figures as a Dynamic Templating Method for Polymers and Nanomaterials, *Adv. Mater.*, 2006, **18**, 973–989.
30 N. Maruyama, *et al.*, Mesoscopic patterns of molecular aggregates on solid substrates, *Thin Solid Films*, 1998, **327–329**, 854–856.
31 C. Rodriguez-rivero, J. R. Castrejón-pita and I. M. Hutchings, Aerodynamic Effects in Industrial Inkjet Printing, *J. Imaging Sci. Technol.*, 2018, **59**, 40401-1–40401-10.
32 M. S. Park and J. K. Kim, Breath figure patterns prepared by spin coating in a dry environment, *Langmuir*, 2004, **20**, 5347–5352.
33 O. Pitois and B. François, Crystallization of condensation droplets on a liquid surface, *Colloid Polym. Sci.*, 1999, **277**, 574–578.
34 E. L. Koschmieder, *Bénard Cells and Taylor Vortices*, Cambridge University Press, 1993.

